

Article

Effect of Sodium Hydroxide, Liquid Sodium Silicate, Calcium Hydroxide, and Slag on the Mechanical Properties and Mineral Crystal Structure Evolution of Polymer Materials

Guodong Huang^{1,2,3,4,*}, Yaqian Li¹, Yuting Zhang^{1,2}, Jielei Zhu^{1,2}, Dawei Li^{1,2} and Bo Wang¹

¹ School of Civil Engineering and Construction, Anhui University of Science and Technology, Huainan 232001, China; yqlia@aust.edu.cn (Y.L.); ytzhang@aust.edu.cn (Y.Z.); jlzhu@aust.edu.cn (J.Z.); dwli@aust.edu.cn (D.L.); bwang@aust.edu.cn (B.W.)

² Hefei Comprehensive National Science Center, Institute of Energy, Hefei 230031, China

³ Institute of Environment-Friendly Materials and Occupational Health, Anhui University of Science and Technology, Wuhu 241003, China

⁴ Fujian Provincial Colleges and University Engineering Research Center of Engineering Quality Inspection and Safety Assessment, Longyan 364000, China

* Correspondence: gdhuang@aust.edu.cn



Citation: Huang, G.; Li, Y.; Zhang, Y.; Zhu, J.; Li, D.; Wang, B. Effect of Sodium Hydroxide, Liquid Sodium Silicate, Calcium Hydroxide, and Slag on the Mechanical Properties and Mineral Crystal Structure Evolution of Polymer Materials. *Crystals* **2021**, *11*, 1586. <https://doi.org/10.3390/cryst11121586>

Academic Editors: Shunbo Zhao, Juntao Ma, Shan Li and Francesco Capitelli

Received: 20 November 2021

Accepted: 15 December 2021

Published: 20 December 2021

Publisher's Note: MDPI stays neutral with regard to jurisdictional claims in published maps and institutional affiliations.



Copyright: © 2021 by the authors. Licensee MDPI, Basel, Switzerland. This article is an open access article distributed under the terms and conditions of the Creative Commons Attribution (CC BY) license (<https://creativecommons.org/licenses/by/4.0/>).

Abstract: To study the key factors that affect the mechanical properties of polymer materials and explore the relationship between mineral crystal formation and strength development, fly ash (FA) polymer samples were prepared using sodium hydroxide, slag, liquid sodium silicate, and hydrated lime as activators. A change in the compressive strength was observed, and X-ray diffraction measurements were carried out to confirm the change. The effects of different types and amounts of activators on the formation and transformation of mineral crystals in FA polymer samples as well as on the development of compressive strength were studied. Moreover, the relationship between the formation and transformation of mineral crystals and the development of compressive strength was established. The results show that the strongly alkaline excitation environment established by sodium hydroxide is the prerequisite for crystal formation and development of compressive strength. Under this strongly alkaline excitation environment, slag, hydrated lime, and liquid sodium silicate can increase the amounts of calcium and silicon, which promote the formation and development of hydrated calcium silicate and hydrated calcium silicoaluminate in polymers and significantly improve the compressive strength.

Keywords: polymer material; crystal; activator; mechanical properties

1. Introduction

The production and application of Portland cement, a traditional building material, are affected by severe issues, including high energy consumption, high degree of pollution, and significant greenhouse gas emissions, which seriously threaten the environment on which society depends. In this context, countries around the world are taking steps to reduce greenhouse gas emissions by limiting the production capacity of heavily polluting industries with high energy consumption in order to meet strict global agreements. China has promised to achieve goals regarding both carbon dioxide peaking and carbon neutrality. In particular, China has promised to hit peak carbon dioxide emissions before 2030, which are then slowly expected to decrease after reaching the peak. Furthermore, carbon dioxide emissions should be offset by tree planting, energy conservation, and emission reduction, and the country aims to achieve carbon neutrality by 2060. Therefore, the production and use of Portland cement will be seriously reduced, thereby forcing scientists to devote their research efforts to new green building materials with low energy consumption, no pollution, and low carbon emissions. Polymer materials have gradually attracted increasing

attention from the scientific community because of their numerous advantages, including a low carbon footprint, good energy-saving properties, and environmental friendliness [1].

Compared with Portland cement, polymer materials constitute a new type of cementitious materials that exhibit multiple advantages [2]. The raw materials used to prepare polymer materials are industrial solid waste materials, such as fly ash (FA), coal gangue powder, and slag powder; thus, the preparation of polymer materials does not require the consumption of nonrenewable resources, such as limestone and clay [3]. Furthermore, polymer materials do not need to be calcined at high temperature, which greatly reduces the consumption of coal and electric energy as well as carbon emissions [4]. Regarding recycling, when polymer materials reach the end of their service life, they can be reused, so as to realize unlimited recycling [5]. Owing to all these advantages, polymer materials are envisaged to replace Portland cement to become the mainstream building materials in the near future.

However, the properties of polymer materials are affected by several disadvantages, which limit their application prospects. First, polymer materials mainly involve the polymerization of silicon–aluminum alloys and formation of the mineral crystals via the polymerization of silicon–oxygen tetrahedra and aluminum–oxygen tetrahedra. The mechanical properties of the polymerization products obtained via the polymerization of silicon–aluminum alloys are poor, which hinders the possibility of replacing Portland cement-based materials with polymer materials [6]. Although steam curing can improve the mechanical properties of polymer materials to a certain extent, this method undoubtedly increases the preparation cost and carbon emissions [7]. Alternatively, the excitation of activators also plays an important role in improving the mechanical properties of polymer materials [8]. This is attributed to the fact that suitable activators can promote the formation of high-strength mineral crystals and lead to the development of compressive strength in polymer materials [9]. Therefore, it is very important to analyze in detail the influence of different types and contents of activators on the formation of different mineral crystals in polymer materials as well as establish the relationship between the formation and transformation of micro mineral crystals and the mechanical properties of polymer materials.

In this study, polymer materials were modified and activated by changing the type and amount of activator with the objective of improving the mechanical properties of polymer materials. X-ray diffraction (XRD) measurements were conducted to analyze the relationship between the formation and transformation of mineral crystals and the mechanical properties of the polymer materials. Furthermore, the influence of the type and content of activator on the formation and transformation of mineral crystals in polymer materials was innovatively investigated, the corresponding relationship between the formation and transformation of mineral crystals and the development of compressive strength was put forward, and finally the influence of the formation and development of different mineral crystals on the establishment and development of compressive strength was obtained. Thus, this study provides methods to further promote the performance improvement of polymer materials.

2. Materials and Methods

2.1. Materials

2.1.1. Fly Ash and Ground-Granulated Blast-Furnace Slag

Primary Fly ash (FA) (Taiyue mineral products Co., Ltd., Shijiazhuang, Hebei, China) was used as the raw material for the preparation of polymer materials. The specific surface area of FA reached $350 \text{ m}^2 \text{ kg}^{-1}$, and the particle fineness reaching the margin of a square-hole sieve ($45 \mu\text{m}$) was less than 18%. Table 1 presents the chemical composition of FA detected by X-ray fluorescence (XRF). Ground-granulated blast-furnace slag (GS) was mainly used as a calcium-increasing agent for preparing the polymer materials; it was provided by a mineral product processing plant in Shijiazhuang, Hebei province. The specific surface area of GS reached $400 \text{ m}^2 \text{ kg}^{-1}$, and the particle fineness reaching the

margin of the square-hole sieve (45 μm) was less than 12%. Its chemical composition is also listed in Table 1.

Table 1. Chemical composition (%).

	SiO ₂	Al ₂ O ₃	Fe ₂ O ₃	CaO	MgO	Na ₂ O	K ₂ O	Others	Loss
Fly ash	53.06	32.93	5.86	2.43	1.12	0.69	1.58	1.79	1.16
Ground-granulated blast-furnace slag	31.35	18.65	0.57	34.65	9.31	1.26	0.84	2.25	0.73

2.1.2. Activators

Sodium hydroxide (NaOH, NH) powder and liquid sodium silicate (Na₂SiO₃, LSS) were used as activators. NH is an analytical reagent. Industrial-grade LSS with purity greater than 95% was used in this study, and Na₂O, SiO₂, and H₂O accounted for 9.68, 25.26, and 65.02% of the total mass, respectively.

2.1.3. Other Materials

Industrial-grade calcium hydroxide (Ca(OH)₂, CH) with purity greater than 95% was employed herein. The specific surface area of CH reached 300 m² kg⁻¹, and the particle fineness reaching the margin of the square-hole sieve (45 μm) was less than 22%. River sand was used for the continuous grading test; its fineness modulus was 2.78. Tap water was used in all the experiments.

2.2. Sample Preparation

2.2.1. Mix Proportions of Samples

The mix proportions of the polymer samples are listed in Table 2. Sample H-1 is the experimental control sample, and only free water was used to excite the polymer materials. Samples H-2 to H-5 were, respectively, mixed with GS, CH, LSS, and NH to excite the FA polymer materials. These samples were used to analyze the effects of different activators on the excitation, formation, and transformation of mineral crystals. Further, under NH excitation, the GS content was gradually increased in samples H-6 to H-8. This resulted in an increased calcium content, and the effects of calcium addition on the mechanical properties and crystal structure of the polymer samples were also analyzed. In samples H-9 and H-10, the contents of calcium and silicon were increased by adding CH and LSS, respectively; these samples were used to test the effect of CH and LSS under the NH excitation.

Table 2. Mix proportion of samples/g.

	Fly Ash	Ground-GRANULATED Blast-Furnace Slag	Ca(OH) ₂	Water	Liquid Sodium Silicate	NaOH	Sand	L/S
H-1	450	/	/	225	/	/	1350	0.5
H-2	405	45	/	225	/	/	1350	0.5
H-3	405	/	45	225	/	/	1350	0.5
H-4	450	/	/	147	120	/	1350	0.5
H-5	450	/	/	225	/	20	1350	0.5
H-6	360	90	/	225	/	20	1350	0.5
H-7	270	180	/	225	/	20	1350	0.5
H-8	180	270	/	225	/	20	1350	0.5
H-9	270	180	/	147	120	20	1350	0.5
H-10	225	180	45	147	120	20	1350	0.5

2.2.2. Sample Preparation and Curing

To illustrate the preparation method of the polymer materials, sample H-10 was considered as a representative example. First, NH and LSS were dissolved in the test water according to the proportions presented in Table 2. Sodium hydroxide was added to the

solution, and the resulting solution was stirred for 30 s. Subsequently, sand was added, and the solution was quickly stirred for 1 min. Finally, the polymer material was poured into a $40 \times 40 \times 160 \text{ mm}^3$ standard mold. The prepared samples were placed in a curing chamber, where the temperature was kept constant at $20 \pm 2 \text{ }^\circ\text{C}$, and the humidity was kept at above 95%. After curing for 3 d, the mold was removed, while the samples remained in the curing chamber until the desired curing time was reached.

2.3. Methods

2.3.1. Compressive Strength Test

A TYE-300 automatic press (Blue standard construction instrument Co., Ltd., Cangzhou, Hebei, China) was used to test the compressive strength of the polymer materials that were cured for 3, 28, and 60 d, respectively. The final results were obtained by averaging the results from six different tests.

2.3.2. X-ray Diffraction Measurements

The polymer samples cured for 28 d were investigated by XRD (Rigaku SmartLab SE intelligent X-ray diffractometer) (Rigaku, Beijing, China) to test the effects of different types and contents of activators on the composition and transformation of the mineral crystal structure of the polymer materials. General test conditions are as follows: X-ray tube: voltage-40 kV, current-30 mA; anode target material: Cu target, $K\alpha$ radiation; measurement angle range (2θ): $5\text{--}70^\circ$. Furthermore, the XRD results were used in combination with the compressive strength data to analyze the relationship between the development of compressive strength and the crystal formation and transformation in the polymer materials.

3. Results and Discussion

3.1. Compressive Strength Analysis

3.1.1. Effect of a Single Activator on the Compressive Strength

(1) Excitation by free water, ground-granulated blast-furnace slag, and calcium hydroxide

When only liquid water was used to mix the FA polymer materials, the mold of sample H-1 could not be removed after curing for 3 d due to its low strength. Unless it was cured for 28 or 60 d, sample H-1 did not exhibit a significant compressive strength. Furthermore, samples H-2 and H-3, which were activated by GS and CH, respectively, did not possess a significant compressive strength even after being cured for 60 d (Figure 1). It can thus be inferred that FA polymer materials do not exhibit compressive strength when activated only by free water, GS, or CH, separately. This also indicates that the addition of free water, GS, or CH cannot promote the polymerization activity of FA.

(2) Excitation by liquid sodium silicate

When only LSS was used as the activator, although the mold of sample H-4 could still not be removed after curing for 3 d, it exhibited a compressive strength of 1.2 MPa after being cured for 28 d, and its compressive strength increased to 1.5 MPa after being cured for 60 d (Figure 1). However, this does not necessarily indicate that LSS has an activation effect on FA as LSS has its own coagulation ability. LSS can induce the generation of compressive strength by absorbing active aluminum from FA and by combining its own active sodium and silicon to form albite. This is the reason why sample H-4 exhibited a very low compressive strength only after being cured for 28 d. This mechanism is further discussed in the XRD results in Section 3.2.4.

(3) Excitation by sodium hydroxide

When NH was used as the activator, the compressive strength of sample H-5 changed markedly. After curing for 3 and 28 d, the compressive strength of sample H-5 reached 1.7 and 4.8 MPa, respectively. The compressive strength increased further to 5.5 MPa after curing for 60 d, which is significantly higher than that obtained for sample H-4 (Figure 1). Different from the cases of excitation by free water, GS, and CH, the NH excitation can effectively stimulate the polymerization activity of FA and induce a considerable com-

pressive strength in the polymer sample. This is attributed to the fact that the addition of NH significantly improves the pH of the reaction environment in polymer materials [10]. However, the addition of free water, GS, and CH cannot result in the pH being > 14 , as required by the polymerization reaction environment. This is the main reason why sample H-5 exhibited a certain degree of compressive strength, while samples H-1 to H-4 did not show any compressive strength. The reaction mechanism of the polymers is discussed in detail in the XRD analysis in Sections 3.2.1 and 3.2.2).

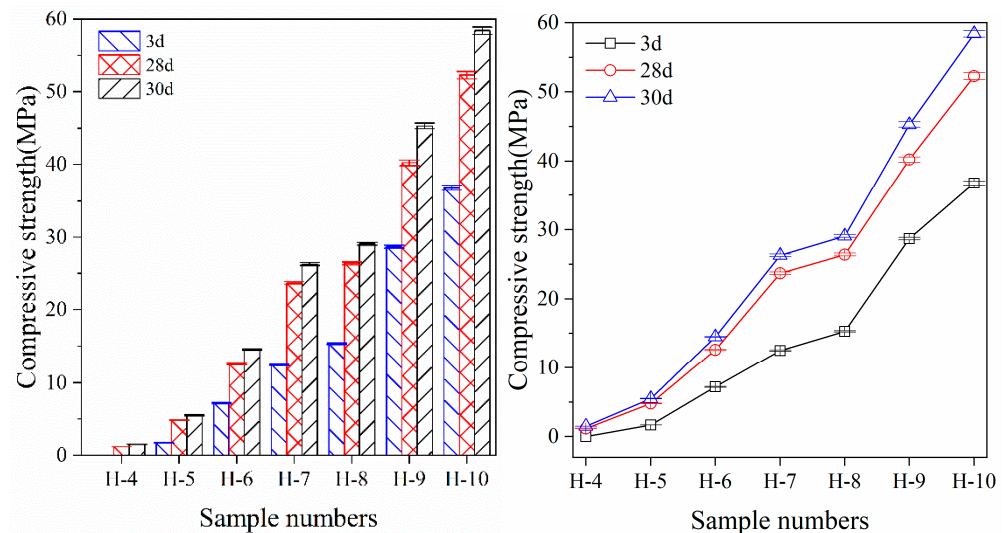


Figure 1. Compressive strength of the polymer samples.

The abovementioned results thus conclude that only NH can induce a highly alkaline excitation environment ($\text{pH} > 14$), which stimulates the polymerization activity of FA, promotes the dissolution and repolymerization process of the active substances, and induces a considerable compressive strength in the polymer samples [11].

3.1.2. Influence of Ground-Granulated Blast-Furnace Slag in the Presence of a Constant Sodium Hydroxide Content on the Compressive Strength

The effect of GS on compressive strength was analyzed for samples H-6 to H-8 using a constant NH content while gradually increasing the GS content.

(1) Ground-granulated blast-furnace slag content of 90 g (20%)

When the NH content was maintained at 20 g but that of GS was increased to 90 g (20%), the compressive strength of sample H-6 after being cured for 3 d increased to 7.2 MPa. This value is higher than that of sample H-5 (without GS addition) by 5.5 MPa, and the growth rate is 323% higher. After curing for 28 and 60 d, the compressive strength of sample H-6 further increased to 12.6 and 14.5 MPa, respectively. These values are higher than those of sample H-5 by 7.8 and 9 MPa, respectively, and the growth rates are 163 and 164% higher, respectively (Figure 1). The addition of GS can significantly improve the compressive strength of FA polymer materials. This also indicates that addition of GS can lead to significant improvement in the reactivity of FA; however, the positive effect of GS could only be observed when the NH amount was at least 20 g. This also shows that a highly alkaline excitation environment is a sufficient condition for polymer materials to acquire improved compressive strength [12].

(2) Ground-granulated blast-furnace slag content of 180 g (40%)

With the increase in the GS content to 180 g (sample H-7), the compressive strength of the sample improved significantly. After curing for 3, 28, and 60 d, the compressive strength of sample H-7 increased to 12.5, 23.7, and 26.3 MPa and was 73.6, 88.1, and 81.4%, respectively, higher than those of sample H-6 for the same curing time (Figure 1). This shows that increasing the GS content results in a significant improvement in the

compressive strength of the FA polymer materials. It also shows that the polymerization activity of FA increases with the increase in the GS content.

(3) Ground-granulated blast-furnace slag content of 270 g (60%)

When the GS content was increased to 270 g (sample H-8), although the compressive strength of the sample continued to increase, the increase was only modest. The compressive strength of sample H-8, after being cured for 3, 28, and 60 d, increased to 15.3, 26.4, and 29.1 MPa and was only 22.4, 11.4, and 10.6%, respectively, higher than those of sample H-7 (Figure 1). This indicates that as the GS content continues to increase, its positive effect on the polymerization activity of FA begins to decrease significantly.

To conclude, GS can enhance the compressive strength only when sufficient NH is added. Furthermore, when the NH content was kept constant at 20 g, the compressive strength of the FA polymer samples first increased markedly and then increased more slowly with the increase in the GS content [13].

3.1.3. Influence of Multiple Activators on the Compressive Strength

(1) Liquid sodium silicate

Although the beneficial effect of GS on the compressive strength is not clear, in the following study, an attempt was made to improve the compressive strength by adding both LSS and CH while keeping the NH and GS contents constant. When the LSS content was 120 g, the compressive strength of sample H-9 increased to 28.7, 40.2, and 45.3 MPa and was 87.6% (after being cured for 3 d), 52.3% (after being cured for 28 d), and 55.7% (after being cured for 60 d) higher than that of sample H-8 (Figure 1). Sample H-4 exhibited a very low compressive strength (less than 2 MPa) when only LSS was added; however, when the NH and GS contents were 20 and 225 g, respectively, the compressive strength of sample H-9 was much higher than that of sample H-8 (without LSS addition). This indicates that LSS can further improve the reactivity of FA; however, this can only occur in a highly alkaline excitation environment (i.e., with sufficient NH addition) and with a sufficient content of added GS (40%). LSS is mainly composed of active silicon; therefore, it can provide the raw materials necessary for polymerization reaction environment [14]. The increase in the active silicon content is conducive to the formation of hydrated calcium silicate and calcium aluminosilicate, which significantly improved the compressive strength of sample H-9, as confirmed by the XRD results.

(2) Calcium hydroxide

When a certain amount of CH (45 g) was added, the compressive strength of sample H-10 increased to 36.8, 52.3, and 58.4 MPa (Figure 1), being 28.2% (after being cured for 3 d), 30.1% (after being cured for 28 d), and 28.9% (after being cured for 60 d) higher than that of sample H-9 (without CH addition). Thus, the addition of CH can also significantly improve the compressive strength of FA polymer samples; however, this can only occur when sufficiently large amounts of NH, GS, and LSS are added. CH is mainly composed of calcium ions. When dissolved in a polymerization environment, CH can provide a large amount of active calcium, which can combine with the active silicon provided by LSS to form hydrated calcium silicate gel [15], thereby significantly improving the compressive strength of sample H-10, as confirmed by the XRD results.

Importantly, the strongly alkaline environment induced by NH, LSS, and CH can increase the silicon and calcium contents, promote the formation of the polymerization products, enhance the polymerization efficiency, improve the formation of high-strength polymerization products, and further improve the compressive strength of the polymer samples.

3.2. X-ray Diffraction Analysis

3.2.1. X-ray Diffraction Analysis of the Raw Materials

(1) X-ray diffraction analysis of ground-granulated blast-furnace slag

Figure 2 shows the XRD patterns of the FA and GS raw materials. Alongside the XRF results (Table 1) for GS, the XRD pattern shows that GS contains a large number of elements, such as calcium, silicon, and aluminum; however, there is no GS characteristic

peak in the XRD pattern, which indicates that GS is predominantly characterized by an amorphous structure. This is attributed to the fact that GS is a glassy substance formed by the melting of silicate and aluminosilicate as the main components when smelting pig iron in a blast furnace, which cannot get crystallized after quenching. Therefore, GS is a raw material with a high polymerization activity.

(2) X-ray diffraction analysis of fly ash

The results presented in Table 1 and the patterns shown in Figure 2 indicate that FA contains a large amount of silicon, aluminum, and other elements; however, the content of calcium is low. This leads to the appearance of quartz peaks (SiO_2 , PDF46-1045: 20.8° , 26.6° , 50.1° , and 64.4°) and mullite peaks ($2\text{Al}_2\text{O}_3 \cdot \text{SiO}_2$, PDF15-0776: 16.4° , 25.9° , 30.9° , 33.1° , 35.2° , 39.3° , 40.9° , 42.6° , and 60.7°) in the XRD pattern. This result is ascribed to the formation of a high-temperature environment that is formed during the coal combustion process (FA is formed after the complete combustion of coal), which promotes the fusion of unburnable active silicon and active aluminum in coal and results in the formation of mullite crystals in FA [16].

(3) X-ray diffraction analysis of sample H-1

When excited by free water, the visible XRD peaks for sample H-1, after being cured for 28 d, are still only those for quartz and mullite. The intensity of the characteristic peaks (quartz and mullite) did not increase, remaining almost the same as that of FA. This shows that free water has no stimulating effect on FA, and FA does not undergo any polymerization, rendering it impossible to form new mineral crystals. This is the main reason why sample H-1 did not exhibit any compressive strength.

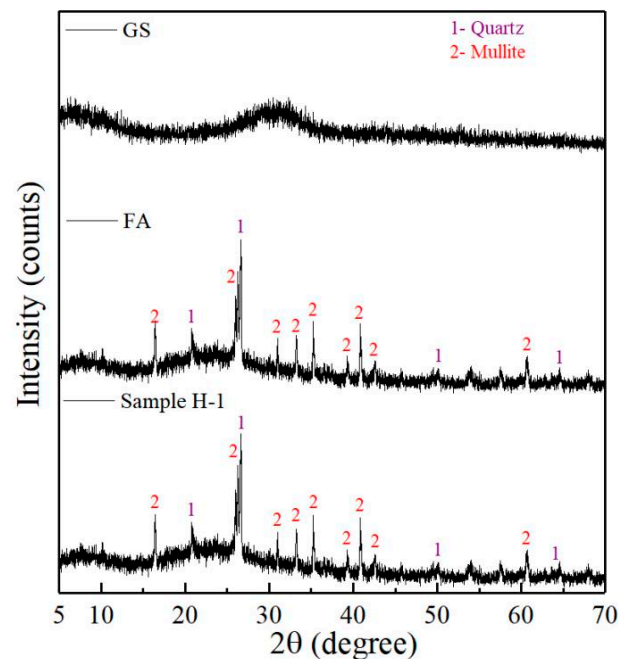


Figure 2. XRD patterns of the raw materials.

3.2.2. X-ray Diffraction Analysis of the Single Activators

(1) X-ray diffraction analysis of sample H-4

The XRD patterns of the polymer samples after single excitation by LSS or NH are shown in Figure 3. When excited by LSS, the characteristic peaks of the quartz and mullite are still visible in the XRD pattern of sample H-4, albeit at a slightly lower angle (26.6° and 25.9°) than those of sample H-1. This shows that a small amount of active silicon and aluminum causes a low degree of polymerization after the addition of LSS. Moreover, pronounced albite ($\text{Na}_2\text{O} \cdot \text{Al}_2\text{O}_3 \cdot 6\text{SiO}_2$, PDF19-1184) characteristic peaks at 21.9° , 24.1° , and 27.6° appeared in the XRD pattern of sample H-4; these peaks were not present in the

XRD pattern of sample H-1. The addition of LSS promotes the activity of active silicon and aluminum in FA as well as the formation of albite, which is also the reason for the very low compressive strength of sample H-4 (1.2 MPa, 28 d) [17]. LSS is mainly composed of active sodium and silicon; therefore, it provides a large number of active substances to the polymerization reaction environment and promotes the reaction activity of active silicon and aluminum in FA [18]. The polymerization of active sodium with aluminum and silicon results in the formation of albite, which is the main reason for the appearance of the albite characteristic peak and the reduction in the intensity of the mullite characteristic peak in the XRD pattern of sample H-4.

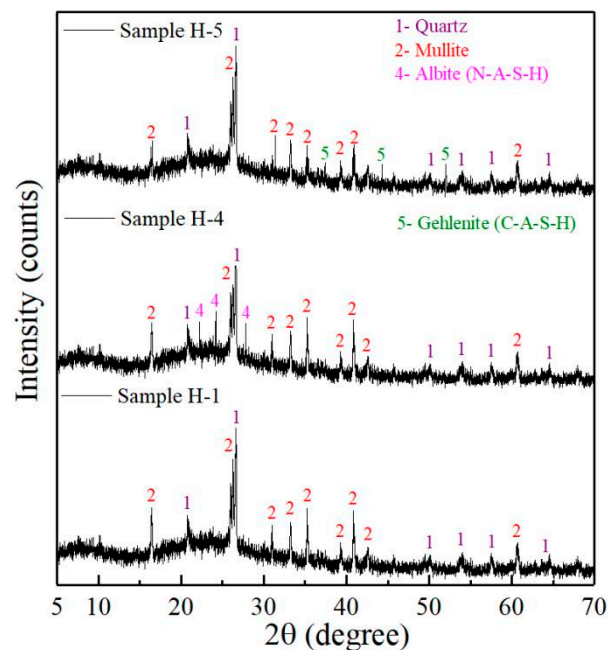


Figure 3. XRD patterns of the single activators.

(2) X-ray diffraction analysis of sample H-5

When excited by NH, the characteristic peaks of mullite at 16.5° , 35.3° , and 40.9° in the XRD pattern of sample H-5 were further reduced compared with those of samples H-1 and H-4. This shows that the amounts of active silicon and aluminum participating in polymerization in sample H-5 are significantly higher than those in samples H-1 and H-4, which indicates that NH exhibits a more pronounced excitation effect than other single activators. Moreover, the XRD pattern of sample H-5 clearly shows the characteristic peaks of gehlenite (PDF 35-0755, 16.5° , 35.3° , and 40.9°); this peak was not visible in the patterns of samples H-1 and H-4. The addition of NH significantly improves the pH and creates a highly alkaline excitation environment, which promotes the gradual activation of silicon, aluminum, and a small amount of calcium in FA [19]. Under the action of a high concentration of OH^- , active calcium polymerizes with silicon and aluminum to form gehlenite [20], which is the main reason for the reduction in the intensity of the characteristic peaks of mullite as well as the appearance of the gehlenite peak in the XRD pattern of sample H-5.

Gehlenite is a hydrated calcium aluminosilicate gel (C-A-S-H) and it is a polymerization product formed by alkali activation, which is the main reason behind the development of the compressive strength for sample H-5 (4.8 MPa, 28 d, 300% higher than that of sample H-4). GS and CH were added during the preparation of samples H-2 and H-3 (0 MPa, 28 d), which also provides a large quantity of active calcium and silicon for the formation of gehlenite. However, samples H-2 and H-3 did not exhibit high compressive strength, even after being cured for a long time. This proves that a prerequisite for polymer materials to exhibit a high compressive strength is a strongly alkaline excitation environment [21].

This is also the reason why samples H-1 to H-3 did not show any compressive strength. Furthermore, the characteristic peak of albite appeared in the XRD pattern of sample H-4 but not in that of sample H-5, which also shows that the polymerization mechanism of sample H-5 is completely different from that of sample H-4. Sample H-4 mainly relies on the polymerization ability of LSS to form albite minerals, but it does not promote the polymerization activity of FA. On the other hand, the strongly alkaline excitation environment of sample H-5 promotes the activity of FA, resulting in the rapid dissolution and polymerization of active calcium, silicon, and aluminum from FA and the formation of gehlenite [22], which induces a high compressive strength.

3.2.3. X-ray Diffraction Analysis of the Effect of Ground-Granulated Blast-Furnace Slag on the Compressive Strength

(1) X-ray diffraction analysis of sample H-6

After having ensured that NH has established a highly alkaline excitation environment, it was observed that the mineral crystals in sample H-6 changed noticeably with the addition of GS. Table 1 and Figure 4 present that when the content of GS was 90 g (20%), the intensities of the characteristic peaks of mullite (35.3° and 40.9°) in the XRD pattern of sample H-6 were significantly higher than those of sample H-5; however, there was no significant change compared with the XRD pattern of sample H-1. This shows that the polymerization efficiency of active silicon and aluminum in FA is reduced after GS addition. Moreover, the intensity of the characteristic peak of gehlenite in the XRD pattern of sample H-6 did not increase significantly compared with that of sample H-5, but anorthite ($\text{CaO}\cdot\text{Al}_2\text{O}_3\cdot 2\text{SiO}_2$, PDF41-1486) characteristic peaks appeared at 22° , 23.5° , and 27.7° . These peaks were not visible in the XRD patterns of samples H-1 to H-5. In a highly alkaline excitation environment, active materials (calcium, silicon, and aluminum) first dissolve quickly from the GS particles and then polymerize to form anorthite [23,24]. Moreover, there also exists a type of hydrated calcium aluminosilicate gel (C-A-S-H) that plays an important role in the development of the compressive strength in FA polymer samples. However, although a certain amount of GS was also added to sample H-2, due to the lack of a highly alkaline excitation environment ($\text{pH} > 14$), GS did not exhibit an excellent polymerization performance. As a result, sample H-2 did not possess a high compressive strength (0 MPa, 28 d). However, in a highly alkaline environment, the polymerization of FA easily produces gehlenite minerals, while GS can easily form anorthite minerals [25]. This is proven by the fact that the characteristic peak of anorthite appeared in the XRD pattern after GS was added to sample H-6, while the characteristic peak of gehlenite appeared only in the XRD pattern of sample H-5.

More importantly, the characteristic peaks of tobermorite ($\text{Ca}_5\text{Si}_6\text{O}_{16}(\text{OH})_2\cdot 4\text{H}_2\text{O}$, PDF45-1480) and hillebrandite ($\text{Ca}_2(\text{SiO}_3)(\text{OH})_2$, PDF42-0538) can be clearly observed in the XRD pattern of sample H-6, while these three characteristic peaks at 18.4° , 29.4° , and 30.4° did not appear in the XRD patterns of samples H-1 to H-5. Tobermorite and hillebrandite are generally considered as a type of hydrated calcium silicate gel (C-S-H) as well as a major product of polymerization [26]. Owing to the poor crystallinity of hydrated calcium silicate gel, it is generally difficult to determine its existence via XRD measurements. Therefore, the formation of calcium silicate gel is usually inferred from the existence of the tobermorite and hillebrandite peaks in the XRD patterns. The addition of GS provides more active calcium and silicon for the polymerization environment. In a strongly alkaline environment, active calcium and silicon continuously dissolve from the GS particles and polymerize to form hydrated calcium silicate gel [27], which plays a key role for the establishment and development of the compressive strength in sample H-6 ((12.6 MPa, 28 d, 163% higher than that of sample H-5)). Therefore, the addition of GS introduces active calcium into the polymer material system, breaks the low-strength polymerization product that originated from the traditional polymer material in an aluminum–silicon alloy, and promotes the formation of high-strength hydrated calcium silicate and hydrated calcium silicoaluminate [28], which significantly improve the compressive strength. However, the

strengthening effect of GS must take place in a strongly alkaline excitation environment ($\text{pH} > 14$).

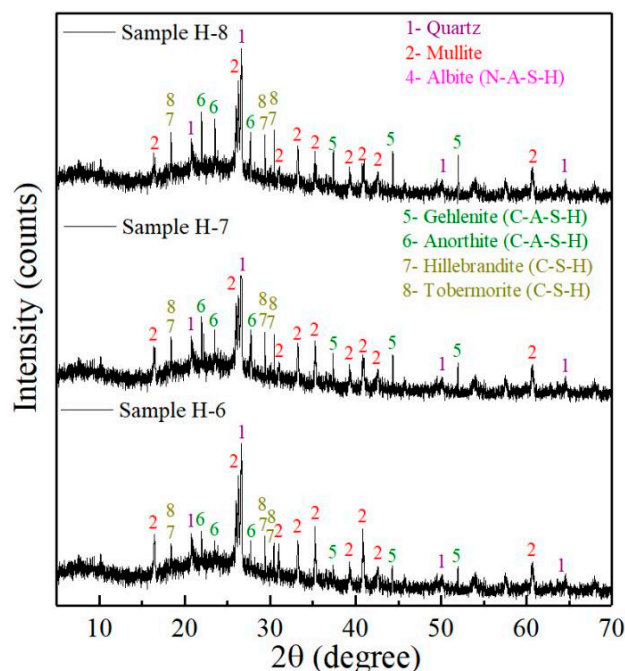


Figure 4. XRD patterns revealing the strengthening effect of GS.

(2) X-ray diffraction analysis of sample H-7

With the increase in the GS content (180 g, 40%), the intensity of the characteristic peaks of the mineral crystals in the XRD pattern of sample H-7 changed significantly compared with those of sample H-6, as shown in Figure 3. The intensities of the characteristic peaks of mullite (16.4° , 31° , 35.2° , and 40.8°) in the XRD pattern of sample H-7 were significantly lower than those of sample H-6. This shows that the amount of FA participating in the polymerization reaction in sample H-7 is significantly increased. Furthermore, it shows that the increase in the GS content can enhance the polymerization activity of FA in a strongly alkaline excitation environment [29]. At the same time, the intensities of the characteristic peaks of gehlenite (16.4° , 31° , 35.2° , and 40.8°) and anorthite (22° , 23.5° , and 27.7°) in the XRD pattern of sample H-7 were significantly higher than those of sample H-6. This indicates that with the increase in the GS content, the contents of active calcium, silicon, and aluminum in the polymerization environment are further increased, which establishes favorable conditions for the formation of gehlenite and anorthite. The increase in the GS content promotes the FA activity, favors the decomposition of mullite in a highly alkaline environment, gives rise to the formation of active silicon and aluminum, and gets polymerized with the active calcium provided by GS to form anorthite [30]. Consequently, as the GS content increased, the intensities of the characteristic peaks of mullite in the XRD pattern of sample H-7 decreased significantly, while the intensities of the characteristic peaks of gehlenite and anorthite increased significantly. Furthermore, the intensities of the characteristic peaks of tobermorite and hillebrandite (18.4° , 29.4° , and 30.4°) in the XRD pattern of sample H-7 were significantly higher than those of sample H-6. This shows that in a highly alkaline reaction environment, as the GS content increases, the crystallinity of the tobermorite and hillebrandite crystals is tremendously improved, which indicates the formation of a larger amount of calcium silicate gel (C-S-H) [31]. Therefore, the increase in the GS content promotes the formation of hydrated calcium silicate and hydrated calcium silicoaluminates, which leads to dramatic improvement in the compressive strength of sample H-7 (23.7 MPa, 28 d, 88.1% higher than that of sample H-6).

(3) X-ray diffraction analysis of sample H-8

When the GS content was increased further to 270 g (60%), the mineral crystal characteristics of sample H-8 changed even more considerably, as shown in Figure 3. First, the intensity of the characteristic peak of mullite at 16.4° in the XRD pattern of sample H-8 was much lower than that of sample H-7, while the intensities of the characteristic peaks at other angles did not decrease significantly. Moreover, the intensity of the anorthite characteristic peak in the XRD pattern of sample H-8 was not significantly higher than that of sample H-7, while the intensities of the gehlenite characteristic peaks (37.4° , 44.3° , and 52.1°) increased to a certain extent. When the GS content was increased from 40 to 60%, the formation of anorthite did not increase further, while that of gehlenite increased slightly. The increase in the GS content inevitably leads to a decrease in the FA content. However, the content of active calcium in GS was significantly higher than that in FA, but the content of active silicon in GS was lower than that in FA (Table 1). This resulted in the significant increase in the content of active calcium in sample H-8, while the content of active silicon continued to decrease [32]. This led to a large amount of active calcium in the polymerization environment without active silicon, which affected the formation of the polymerization products and finally prevented the increase in the formation of anorthite.

However, gehlenite was formed through the combination of active calcium in GS and active silicon along with aluminum in FA. The increase in the GS content could still continue to enhance the reaction activity of FA. However, due to the decrease in the active silicon content in the polymerization environment, the formation of gehlenite only showed a slight increase. As a result, the intensity of the characteristic peak of gehlenite increased slightly, while that of anorthite did not increase. Moreover, the intensities of the characteristic peaks of tobermorite and hillebrandite at 30.4° in sample H-8 were only slightly higher than those in sample H-7. This indicates that the formation of tobermorite and hillebrandite was also seriously affected by the lack of active silicon in the polymerization reaction, resulting in a significant increase in the amount of active calcium, while the amount of calcium silicate gel did not increase significantly. As a result, the intensities of the tobermorite and hillebrandite peaks did not increase significantly. Therefore, the formation of calcium silicate hydrate and hydrated calcium aluminosilicate gel in sample H-8 could not be continuously increased by increasing the GS content (26.4 MPa, 28 d, only 11.4% higher than that of sample H-7) [33]. Thus, the rate at which the compressive strength increased was significantly reduced upon continuously increasing the GS content in the same proportion.

3.2.4. X-ray Diffraction Analysis of the Compound Activators

(1) X-ray diffraction analysis of sample H-9

With the addition of LSS or CH, the mineral crystal composition in polymer samples develops in a more powerful direction, as shown in Figure 5. With the addition of LSS (120 g), the intensities of the characteristic peaks of the quartz (26.6°) and mullite (16.4° , 25.9° , 33.1° , 35.2° , and 40.9°) crystals in the XRD pattern of sample H-9 decreased significantly compared with those of sample H-8. This shows that the polymerization activity of quartz and mullite in FA was further improved after the addition of LSS. Furthermore, the intensities of the characteristic peaks of gehlenite (36.9° , 44.3° , and 52.1°) in the XRD pattern of sample H-9 were significantly higher than those of sample H-8, and a new characteristic peak of gehlenite appeared at 47.2° in the XRD pattern of sample H-9. This indicates that with the incorporation of LSS, the amount of calcium silicate gel formed in H-9 increased significantly, and this conclusion is further confirmed by the fact that the characteristic peaks of anorthite (22° , 23.5° , and 27.7°) in the XRD pattern of sample H-9 were significantly more intense than those of sample H-8. More importantly, the characteristic peaks of tobermorite and hillebrandite (18.4° , 29.4° , and 30.4°) in the XRD pattern of sample H-9 were significantly more intense than those of sample H-8. Moreover, for sample H-9, new tobermorite characteristic peaks appeared at 45.1° , 49.4° , and 54.9° , and a new hillebrandite characteristic peak appeared at 49.4° . This shows that with the addition of LSS, the formation of hydrated calcium silicate and hydrated calcium silicoaluminate in sample H-9 increased significantly, which is also the main reason for

the considerable improvement in the compressive strength (40.2 MPa, 28 d, 52.3% higher than that of sample H-8). The addition of LSS introduces a large amount of active silicon into the polymerization reaction environment and alleviates the issues associated with the excessive active calcium content and the insufficient active silicon content caused by the continuous increase in the GS content [34]. However, the reinforcing effect of LSS could only occur in a strongly alkaline polymerization environment. This is confirmed by the fact that sample H-4 did not exhibit a good compressive strength when only LSS was added.

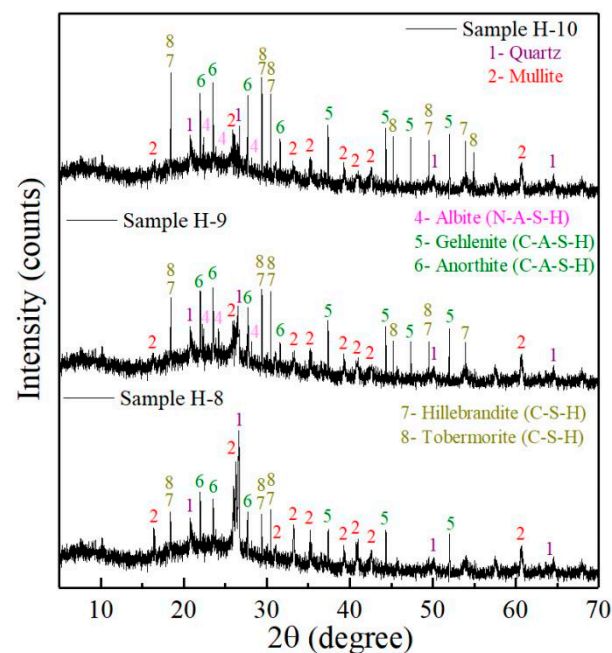


Figure 5. XRD patterns of the compound activators.

(2) X-ray diffraction analysis of sample H-10

With the addition of CH (45 g), the intensities of the characteristic peaks of quartz and mullite crystals in the XRD pattern of sample H-10 did not reduce further compared with those of sample H-9. This shows that the addition of CH did not further improve the polymerization activity of FA. However, the intensity of the characteristic peak of gehlenite in the XRD pattern of sample H-10 was higher than that of sample H-9, but the growth range was not clear. Moreover, the intensities of the characteristic peaks of anorthite (22° , 23.5° , and 27.7°) in the XRD pattern of sample H-10 were significantly higher than those of sample H-9, which shows that the addition of CH remarkably promotes the formation of hydrated calcium silicoaluminates. Furthermore, the intensities of the tobermorite and hillebrandite characteristic peaks in the XRD pattern of sample H-10 were significantly higher than those in sample H-9, and a new tobermorite characteristic peak appeared at 54.9° , which indicates that the formation of calcium silicate gel was also significantly improved. The addition of CH can further promote the formation of calcium silicate hydrate and hydrated calcium aluminosilicate gel [35], which favors the significant improvement in the compressive strength of sample H-10 (52.3 MPa, 28 d, 30.1% higher than that of sample H-9). The addition of LSS leads to a significant increase in the content of active silicon in the polymerization environment. LSS exists in a liquid form; the active silicon contained can directly participate in the polymerization reaction [36]. However, the active calcium obtained in GS and FA can be continuously dissolved from the inside of the GS and FA particles only under strongly alkaline excitation conditions. This leads to a situation in which the active silicon content is too high, and the active calcium content is clearly insufficient in the initial stages of polymerization [37]. The addition of CH compensates for this deficiency because the active calcium contained in CH can be directly released into the polymerization environment through dissolution, which alleviates the issue of the slow

dissolution process of active calcium in GS and FA [38–40]. Therefore, the addition of CH provides active calcium for the polymerization environment and significantly increases the formation volume of calcium silicate hydrate and hydrated calcium aluminosilicate gels. As a result, the characteristic peaks of gehlenite, anorthite, tobermorite, and hillebrandite in the XRD pattern of sample H-10 were considerably more intense.

4. Conclusions

In this study, fly ash polymer samples were prepared using sodium hydroxide (NH), slag (GS), liquid sodium silicate (LSS), and hydrated lime (CH) as activators. X-ray diffraction measurements were conducted to analyze the relationship between the formation and transformation of mineral crystals and the mechanical properties of the polymer materials. Based on the results, following conclusions can be drawn:

- (1) The strongly alkaline excitation environment established by the addition of NH is a sufficient condition for the polymerization of polymer materials and the formation of new mineral crystals. It is also a prerequisite to ensure that the addition of GS, LSS, and CH can continue to enhance the formation of mineral crystals in polymer materials.
- (2) The addition of GS and the increase in its content can not only promote the polymerization activity of FA but also provide large amounts of active calcium, silicon, and aluminum for the polymerization environment, which promotes the formation of hydrated calcium silicate (tobermorite and hillebrandite) and hydrated calcium silicoaluminate (gehlenite and anorthite) and significantly improves the compressive strength. However, an increase in the GS content above 40% leads to the lack of active silicon in the polymerization environment, which hinders the formation of the polymerization products as well as the enhancement in the compressive strength.
- (3) The addition of LSS can alleviate the issues associated with the insufficient active silicon content caused by the increase in GS content; it can thus further promote the formation of the polymerization products, thereby improving the compressive strength of polymer samples.
- (4) The addition of CH can limit the slow dissolution of active calcium in GS and FA, provide active calcium for the polymerization reaction environment more efficiently, promote the formation of the polymerization products, and significantly improve the compressive strength.

Author Contributions: Validation, B.W.; formal analysis, J.Z.; investigation, D.L.; resources, Y.Z.; data curation, Y.L.; writing—original draft preparation, G.H.; writing—review and editing, G.H. All authors have read and agreed to the published version of the manuscript.

Funding: This research was funded by the Funding Project of a key research project of the Natural Science in Colleges and the universities of Anhui Province (KJ2020A0295). Funding also from the Research Foundation of the Institute of Environment-friendly Materials and Occupational Health (Wuhu), Anhui University of Science and Technology (ALW2021YF01), as well as from the Fujian Provincial Colleges and University Engineering Research Center of Engineering quality inspection and safety assessment (LYGF-202001).

Institutional Review Board Statement: Not applicable.

Informed Consent Statement: Not applicable.

Acknowledgments: The research described in this paper was financially supported by the Funding Project of a key research project of the Natural Science in Colleges and the universities of Anhui Province (KJ2020A0295). Funding also from the Research Foundation of the Institute of Environment-friendly Materials and Occupational Health (Wuhu), Anhui University of Science and Technology (ALW2021YF01), as well as from the Fujian Provincial Colleges and University Engineering Research Center of Engineering quality inspection and safety assessment (LYGF-202001).

Conflicts of Interest: The authors declare no conflict of interest.

References

1. Provis, J.L.; Palomo, A.; Shi, C. Advances in understanding alkali-activated materials. *Cem. Concr. Res.* **2015**, *78*, 110–125. [[CrossRef](#)]
2. Luukkonen, T.; Abdollahnejad, Z.; Yliniemi, J.; Kinnunen, P.; Illikainen, M. One-part alkali-activated materials: A review. *Cem. Concr. Res.* **2018**, *103*, 21–34. [[CrossRef](#)]
3. Puertas, F.; González-Fonteboa, B.; González-Taboada, I.; Alonso, M.M.; Torres-Carrasco, M.; Rojo, G.; Martínez-Abella, F. Alkali-activated slag concrete: Fresh and hardened behavior. *Cem. Concr. Compos.* **2018**, *85*, 22–31. [[CrossRef](#)]
4. Huang, G.; Ji, Y.; Li, J.; Hou, Z.; Jin, C. Use of slaked lime and Portland cement to improve the resistance of MSWI bottom ash-GBFS geopolymers against carbonation. *Constr. Build. Mater.* **2018**, *166*, 290–300. [[CrossRef](#)]
5. Shi, C.; Fernández-Jiménez, A.; Palomo, A. New cements for the 21st century: The pursuit of an alternative to Portland cement. *Cem. Concr. Res.* **2011**, *41*, 750–763. [[CrossRef](#)]
6. Hanjitsuwan, S.; Hunpratub, S.; Thongbai, P.; Maensiri, S.; Sata, V.; Chindaprasirt, P. Effects of NaOH concentrations on physical and electrical properties of high calcium fly ash geopolymer paste. *Cem. Concr. Compos.* **2014**, *45*, 9–14. [[CrossRef](#)]
7. Huang, G.; Ji, Y.; Li, J.; Hou, Z.; Dong, Z. Improving strength of calcinated coal gangue geopolymer mortars via increasing calcium content. *Constr. Build. Mater.* **2018**, *166*, 760–768. [[CrossRef](#)]
8. Tuyan, M.; Andiç-Çakır, Ö.; Ramyar, K. Effect of alkali activator concentration and curing condition on strength and microstructure of waste clay brick powder-based geopolymer. *Compos. Part B* **2018**, *135*, 242–252. [[CrossRef](#)]
9. Huang, G.; Ji, Y.; Li, J.; Zhang, L.; Liu, X.; Liu, B. Effect of activated silica on polymerization mechanism and strength development of MSWI bottom ash alkali-activated mortars. *Constr. Build. Mater.* **2019**, *201*, 90–99. [[CrossRef](#)]
10. Cristelo, N.; Tavares, P.; Lucas, E.; Miranda, T.; Oliveira, D. Quantitative and qualitative assessment of the amorphous phase of a Class F fly ash dissolved during alkali activation reactions-effect of mechanical activation, solution concentration and temperature. *Compos. Part B* **2016**, *103*, 1–14. [[CrossRef](#)]
11. He, R.; Ma, H.; Hafiz, R.B.; Fu, C.; Jin, X.; He, J. Determining porosity and pore network connectivity of cement-based materials by a modified non-contact electrical resistivity measurement: Experiment and theory. *Mater. Des.* **2018**, *156*, 82–92. [[CrossRef](#)]
12. Plusquellec, G.; Geiker, M.R.; Lindgård, J.; Duchesne, J.; Fournier, B.; DeWeerd, K. Determination of the pH and the free alkali metal content in the pore solution of concrete: Review and experimental comparison. *Cem. Concr. Res.* **2017**, *96*, 13–26. [[CrossRef](#)]
13. Huang, G.; Ji, Y.; Zhang, L.; Li, J.; Hou, Z. The influence of curing methods on the strength of MSWI bottom ash-based alkali-activated mortars: The role of leaching of OH⁻ and free alkali. *Constr. Build. Mater.* **2018**, *186*, 978–985. [[CrossRef](#)]
14. Temuujin, J.; Van Riessen, A.; Williams, R. Influence of calcium compounds on the mechanical properties of fly ash geopolymer pastes. *J. Hazard. Mater.* **2009**, *167*, 82–88. [[CrossRef](#)]
15. Bignozzi, M.C.; Manzi, S.; Natali, M.E.; Rickard, W.D.; van Riessen, A. Room temperature alkali activation of fly ash: The effect of Na₂O/SiO₂ ratio. *Constr. Build. Mater.* **2014**, *69*, 262–270. [[CrossRef](#)]
16. Yu, C.; Wu, Q.; Yang, J. Effect of seawater for mixing on properties of potassium magnesium phosphate cement paste. *Constr. Build. Mater.* **2017**, *155*, 217–227. [[CrossRef](#)]
17. Bernal, S.A. Effect of the activator dose on the compressive strength and accelerated carbonation resistance of alkali silicate-activated slag/metakaolin blended materials. *Constr. Build. Mater.* **2015**, *98*, 217–226. [[CrossRef](#)]
18. Maraghechi, H.; Rajabipour, F.; Pantano, C.G.; Burgos, W.D. Effect of calcium on dissolution and precipitation reactions of amorphous silica at high alkalinity. *Cem. Concr. Res.* **2016**, *87*, 1–13. [[CrossRef](#)]
19. Sun, Z.; Vollpracht, A. Isothermal calorimetry and in-situ XRD study of the NaOH activated fly ash, metakaolin and slag. *Cem. Concr. Res.* **2018**, *103*, 110–122. [[CrossRef](#)]
20. Bernal, S.A.; de Gutiérrez, R.M.; Pedraza, A.L.; Provis, J.L.; Rodriguez, E.D.; Delvasto, S. Effect of binder content on the performance of alkali-activated slag concretes. *Cem. Concr. Res.* **2011**, *41*, 1–8. [[CrossRef](#)]
21. Bernal, S.A.; Provis, J.L.; Brice, D.G.; Kilcullen, A.; Duxson, P.; van Deventer, J.S. Accelerated carbonation testing of alkali-activated binders significantly underestimates service life: The role of pore solution chemistry. *Cem. Concr. Res.* **2012**, *42*, 1317–1326. [[CrossRef](#)]
22. Bernal, S.A.; Provis, J.L.; Walkley, B.; Nicolas, R.S.; Gehman, J.D.; Brice, D.G.; Kilcullen, A.R.; Duxson, P.; van Deventer, J.S.J. Gel nanostructure in alkali-activated binders based on slag and fly ash, and effects of accelerated carbonation. *Cem. Concr. Res.* **2013**, *53*, 127–144. [[CrossRef](#)]
23. Wu, Q.; Li, X.; Xu, J.; Wang, G.; Shi, W.; Wang, S. Size Distribution Model and Development Characteristics of Corrosion Pits in Concrete under Two Curing Methods. *Materials* **2019**, *20*, 1846. [[CrossRef](#)]
24. He, R.; Ye, H.; Ma, H.; Fu, C.; Jin, X.; Li, Z. Correlating the Chloride Diffusion Coefficient and Pore Structure of Cement-Based Materials Using Modified Noncontact Electrical Resistivity Measurement. *J. Mater. Civ. Eng.* **2019**, *31*, 04019006. [[CrossRef](#)]
25. Huang, G.; Ji, Y.; Zhang, L.; Li, J.; Hou, Z. Advances in Understanding and Analyzing the Anti-diffusion Phenomenon in Complete Carbonation Zone of MSWI Bottom Ash-based Alkali-activated Concrete. *Constr. Build. Mater.* **2018**, *186*, 1072–1081. [[CrossRef](#)]
26. Puertas, F.; Palacios, M.; Manzano, H.; Dolado, J.S.; Rico, A.; Rodríguez, J. A model for the C-A-S-H gel formed in alkali-activated slag cements. *J. Eur. Ceram. Soc.* **2011**, *31*, 2043–2056. [[CrossRef](#)]
27. He, R.; Fu, C.; Ma, H.; Ye, H.; Jin, X. Prediction of Effective Chloride Diffusivity of Cement Paste and Mortar from Microstructural Features. *J. Mater. Civ. Eng.* **2020**, *32*, 04020211. [[CrossRef](#)]

28. Bernal, S.A.; De Gutierrez, R.M.; John, L.P.; Rose, V. Effect of silicate modulus and metakaolin incorporation on the carbonation of alkali silicate-activated slags. *Cem. Concr. Res.* **2010**, *40*, 898–907. [[CrossRef](#)]
29. Walkley, B.; Nicolas, R.S.; Sani, M.-A.; Bernal, S.A.; Van Deventer, J.S.J.; Provis, J.L. Structural evolution of synthetic alkali-activated CaO-MgO-Na₂O-Al₂O₃-SiO₂ materials is influenced by Mg content. *Cem. Concr. Res.* **2017**, *99*, 155–171. [[CrossRef](#)]
30. Li, C.; Sun, H.; Li, L. A review: The comparison between alkali-activated slag (Si+Ca) and metakaolin (Si+Al) cements. *Cem. Concr. Res.* **2010**, *40*, 1341–1349. [[CrossRef](#)]
31. Meller, N.; Kyritsis, K.; Hall, C. The mineralogy of the CaO-Al₂O₃-SiO₂-H₂O (CASH) hydroceramic system from 200 to 350 °C. *Cem. Concr. Res.* **2009**, *39*, 45–53. [[CrossRef](#)]
32. Wang, W.-C.; Wang, H.-Y.; Lo, M.-H. The fresh and engineering properties of alkali activated slag as a function of fly ash replacement and alkali concentration. *Constr. Build. Mater.* **2015**, *84*, 224–229. [[CrossRef](#)]
33. Jin, L.; Huang, G.; Li, Y.; Zhang, X.; Ji, Y.; Xu, Z. Positive Influence of Liquid Sodium Silicate on the Setting Time, Polymerization, and Strength Development Mechanism of MSWI Bottom Ash Alkali-Activated Mortars. *Materials* **2021**, *14*, 1927. [[CrossRef](#)]
34. Ryu, G.S.; Lee, Y.B.; Koh, K.T.; Chung, Y.S. The mechanical properties of fly ash-based geopolymer concrete with alkaline activators. *Constr. Build. Mater.* **2013**, *47*, 409–418. [[CrossRef](#)]
35. Huang, G.; Ji, Y.; Zhang, L.; Hou, Z.; Zhang, L.; Wu, S. Influence of calcium content on structure and strength of MSWI bottom ash-based geopolymer. *Mag. Concr. Res.* **2019**, *71*, 362–372. [[CrossRef](#)]
36. Huang, G.; Yuan, L.; Ji, Y.; Liu, B.; Xu, Z. Cooperative action and compatibility between Portland cement and MSWI bottom ash alkali-activated double gel system materials. *Constr. Build. Mater.* **2019**, *209*, 445–453. [[CrossRef](#)]
37. Huang, G.; Yang, K.; Chen, L.; Lu, Z.; Sun, Y.; Zhang, X.; Feng, Y.; Ji, Y.; Xu, Z. Use of pretreatment to prevent expansion and foaming in highperformance MSWI bottom ash alkali-activated mortars. *Constr. Build. Mater.* **2020**, *245*, 118471. [[CrossRef](#)]
38. Huang, G.; Yang, K.; Sun, Y.; Lu, Z.; Zhang, X.; Zuo, L.; Feng, Y.; Qian, R.; Qi, Y.; Ji, Y.; et al. Influence of NaOH content on the alkali conversion mechanism in MSWI bottom ash alkali-activated mortars. *Constr. Build. Mater.* **2020**, *248*, 118582. [[CrossRef](#)]
39. Ahmari, S.; Zhang, L.; Zhang, J. Effects of activator type/concentration and curing temperature on alkali-activated binder based on copper mine tailings. *J. Mater. Sci.* **2012**, *47*, 5933–5945. [[CrossRef](#)]
40. Singh, J.; Singh, S.P. Development of Alkali-activated Cementitious Material using Copper Slag. *Constr. Build. Mater.* **2019**, *211*, 73–79. [[CrossRef](#)]